OPEN ACCESS

University of BRISTOL

Simplicio, P. V. M., Marcos, A., Joffre, E., Zamaro, M., & Silva, N. (2017). *A systematic performance-oriented tuning for space exploration descent & landing*. Paper presented at Eucass - 7th European Conference for Aeronautics and Space Sciences.

Peer reviewed version

Link to publication record in Explore Bristol Research
PDF-document

University of Bristol - Explore Bristol Research
General rights

This document is made available in accordance with publisher policies. Please cite only the published version using the reference above. Full terms of use are available:
http://www.bristol.ac.uk/red/research-policy/pure/user-guides/ebr-terms/

DOI:

A Systematic Performance-oriented Tuning for Space Exploration Descent & Landing Guidance*

Pedro Simplício⋆†, *Andrés Marcos*⋆, *Eric Joffre*⋆⋆, *Mattia Zamaro*⋆⋆ *and Nuno Silva*⋆⋆
⋆*Technology for Aerospace Control Group, University of Bristol*
University Walk, Bristol BS8 1TR, UK
pedro.simplicio/andres.marcos @bristol.ac.uk
⋆⋆*Airbus Defence and Space Ltd*
Gunnels Wood Road, Stevenage SG1 2AS, UK
eric.joffre/mattia.zamaro.external/nuno.silva @airbus.com
†Corresponding author

Abstract

Descent & landing (D&L) on planetary bodies are scientifically rewarding exploration missions but they are technically challenging due to the complex and poorly-known environment around those bodies. The standard guidance synthesis approach considers nominal conditions and applies optimal control theory to obtain guidance law gains, followed by intensive verification and validation. In this article, it is shown that the standard approach may yield gains that are not optimal once dispersions (and/or other optimal metrics) are taken into account and a tuning approach is then proposed based on *a priori* methodological system assessment. The proposed approach employs systematic high-fidelity simulations to generate trade-off maps on ground that can be uploaded once the spacecraft approaches the target, with its actual conditions in mind. This also provides a valuable understanding of the system dynamics towards the application of other industry-oriented tools including structured $\mathcal{H}_\infty$ optimisation. It is shown that this approach enables propellant consumption reductions of around 40% compared to state-of-practice tuning selections.

1. Introduction

A renewed scientific interest has been growing in the exploration of small asteroids in addition to larger planetary bodies such as Mars, since their weaker gravitational field makes them more easily accessible. However, these exploration missions are very challenging from an engineering perspective, particularly if the natural dynamics in the vicinity of the target asteroid is exploited to alleviate descent & landing (D&L) propellant consumption requirements. This is because small planetary bodies are typically characterised by highly irregular and poorly-known shapes, which render their physical environment extremely uncertain and variable. Moreover, due to the interplanetary distances involved, fully autonomous guidance algorithms are required to cope with communication delays and spacecraft subsystems degradation, as demonstrated by the European Rosetta mission. For all above reasons, the Space community has recognised the need for robust D&L architectures.

As part of the UK Space Agency National Space Technology Programme, the University of Bristol and Airbus Defence and Space were awarded the project entitled "Robust and Nonlinear Guidance and Control for Landing on Small Bodies", with the aim to investigate the application of advanced robust techniques for the design and optimisation of D&L approaches. Although a generic framework is pursued, the project focused on the Martian moon Phobos, which is among the candidates for an interplanetary sample return mission, not only because of the wide interest to solve the unknowns about its formation, but also as a technological precursor for future exploration missions of the Martian System.

Within the project, state-of-practice surveys for Space guidance as well as Space control (which are rather distinct fields in Space) were carried out to provide understanding and assess commonalities. It is noted that typically a successful guidance tuning is translated into an acceptable *trade-off* between allowable position and velocity errors

*This work is funded by the UK Space Agency through a 2016 NSTP-2 Space Technology Fast Track grant entitled "Robust and Nonlinear Guidance and Control for Landing on Small Bodies". Mr. Simplício is also the recipient of a Doctoral Training Partnership award by the Engineering and Physical Sciences Research Council.

Copyright © 2017 by Simplício *et al.* Published by the EUCASS association with permission.

versus propellant consumption or ΔV needed for the manoeuvre. Using results from optimal control theory, optimal conditions can be analytically derived for most of the surveyed techniques.[7,8]

Nevertheless, these conditions are only practical under the assumption of simplified and *well-known* gravitational fields. From the state-of-practice surveys a reconciliation, in exactitude an underlying parametric generalisation, of the D&L techniques was identified.[13] Although this parametrisation seems to be a simple step, it enabled to identify the possibility of applying systematic tuning methodologies, which may prove to be a paradigm change in the current state of practice for Space D&L guidance and control.

In this paper, a systematic tuning methodology that relies on the identified parametric generalisation is presented and applied to Phobos D&L guidance tuning. This approach employs a methodological evaluation of the high-fidelity model over the parameter space to generate *trade-off maps* that enable a clear performance quantification of candidate guidance solutions. In addition, this approach provides a valuable understanding of the system dynamics that supports the future application of other methodologies envisaged in the project, including structured $\mathcal{H}_\infty$ optimisation.[1,6] With this in mind, the paper begins in Sec. 2 with an introduction of the D&L problem and benchmark, followed by the description and application of the tuning methodology using systematic simulation in Sec. 3 and by its reconciliation with structured $\mathcal{H}_\infty$ optimisation in Sec. 4.

2. D&L Problem and benchmark

The generic planetary D&L problem configuration is depicted in Fig. 1 for planar motion but without loss of generality. It describes a spacecraft approaching a moving (small) body target subject to the influence of another (large) body. For this problem, it is assumed that the spacecraft has a dedicated attitude control system that maintains a nadir pointing during the descent (it is actually a requirement of visual-navigation systems). Coupling effects are then considered at actuator level by reserving a fraction of the available thruster authority (10 to 20%) for attitude control.

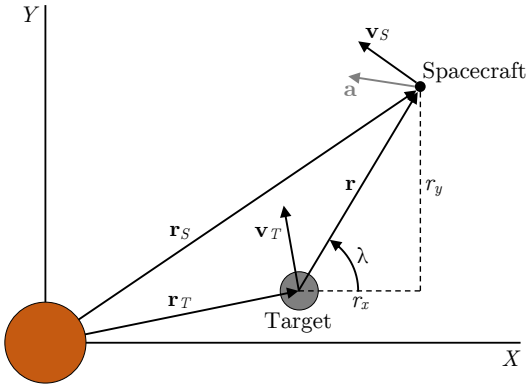

Figure 1: Problem geometry

Based on this figure, the D&L problem lies on the computation of the acceleration input $\mathbf{a}(t)$ between initial and final times, i.e., $t = t_0$ and $t = t_f$, that must be able to:

- Bring the relative position and velocity from the initial boundary conditions $\mathbf{r}(t_0) = \mathbf{r}_0$ and $\mathbf{v}(t_0) = \mathbf{v}_0$ to the final conditions $\mathbf{r}(t_f) = \mathbf{r}_f$ and $\mathbf{v}(t_f) = \mathbf{v}_f$;
- Cope with the effect of uncertainties and external perturbations.

In this problem, the duration from a given instant of time t until the end of the manoeuvre is known as time-to-go, $t_{\text{go}}(t) = t_f - t$, the norm of the relative vector between spacecraft $\mathbf{v}_S(t)$ and target velocities $\mathbf{v}_T(t)$ is known as closing speed and is given by $V_c(t) = \|\mathbf{v}_S(t) - \mathbf{v}_T(t)\|$ and finally the unit vector from target to spacecraft is known as line-of-sight $\mathbf{\Lambda}(t) = \mathbf{r}(t)/\|\mathbf{r}(t)\|$. In addition, and specially important to reconcile the guidance laws addressed in this paper, the concept of zero-effort errors[4] must be introduced:

- Zero-effort-miss (ZEM) is the position error at the end-of-mission if no manoeuvres are made after time t:

$$\mathbf{ZEM}(t) = \mathbf{r}_f - \mathbf{r}(t_f) \mid \mathbf{a}(\tau) = 0 \;\forall\; \tau \in [t, t_f] \tag{1}$$

- Zero-effort-velocity (ZEV) is the velocity error at the end-of-mission if no manoeuvres are made after time t:

$$\mathbf{ZEV}(t) = \mathbf{v}_f - \mathbf{v}(t_f) \mid \mathbf{a}(\tau) = 0 \;\forall\; \tau \in [t, t_f] \tag{2}$$

To obtain analytical expressions for ZEM and ZEV, the (apparent) gravity is typically assumed to be known as an explicit function of time. However, as gravity is more generally given as a function of position, the computation of ZEM and ZEV has to be approximated or performed numerically.[8] For further details on the planetary D&L problem, the reader is referred to Simplício *et al.*[13]

2.1 High-fidelity dynamics in the vicinity of Phobos

Landing on Phobos is particularly challenging because of its reduced mass (8 orders of magnitude smaller than Mars) and proximity to the red planet (mean orbital altitude about 6000 km), which causes the planet's sphere of influence to end just 3.5 km above Phobos' surface (Fig. 2a). Hence, there is no possibility for Keplerian orbits around Phobos and the third-body perturbation of Mars cannot be neglected.

Furthermore, due to the irregular shape and mass distribution of Phobos, the gravity of the moon cannot be accurately accounted for by a spherical field, thus it has to be described using a gravity harmonics (GH) model (Fig. 2b). In this case, using spherical coordinates (r, θ, ϕ) for distance to barycentre, co-latitude and longitude, as well as R for a reference radius and μ_g for the gravitational constant, the gravity potential is given by:

$$U_\mathrm{g}(r,\theta,\phi) = \frac{\mu_\mathrm{g}}{R}\sum_{n=0}^{\bar{n}}\left(\frac{R}{r}\right)^{n+1}\sum_{m=0}^{n} C_n^m(\phi)P_n^m(\cos\theta) \tag{3}$$

where $P_n^m(x)$ are the associated Legendre polynomials and:

$$C_n^m(\phi) = C_{n,m}\cos m\phi + S_{n,m}\sin m\phi \tag{4}$$

is the expansion of the GH coefficients $C_{n,m}$ and $S_{n,m}$. For Phobos, $\bar{n} = 4$ (leading to to 28 coefficients) is assumed to suffice. However, from these coefficients, 19 are highly inaccurately known. In fact, for the work in this article, each coefficient is assumed affected by a Gaussian dispersion with standard deviation equal to its mean value.

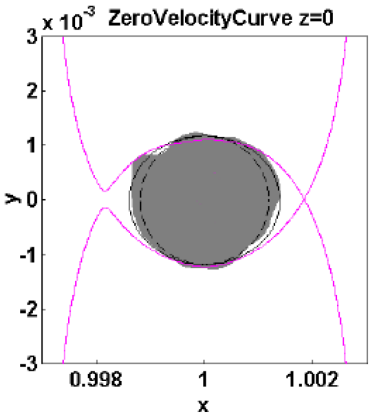

(a) Mars' sphere of influence around Phobos

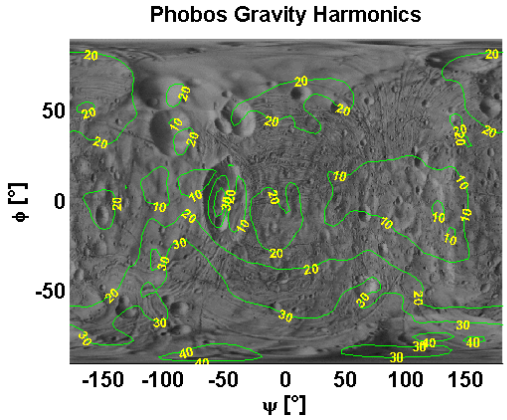

(b) Difference of gravitational acceleration between gravity harmonics and Keplerian model

Figure 2: Highly inhomogeneous gravitational field of Phobos

Given the small eccentricity of Phobos' orbit around Mars (approximately 0.015), the nonlinear dynamics of a spacecraft in the vicinity of the Mars-Phobos system is typically described as a circular restricted three-body problem. In this case, its motion can be written in a body-centred body-fixed (BCBF) frame with origin at the moon's barycentre as:

$$\begin{bmatrix}\dot{\mathbf{r}}(t)\\ \dot{\mathbf{v}}(t)\\ \dot{\nu}(t)\end{bmatrix} = \mathbf{f}\left(\mathbf{r}(t),\mathbf{v}(t),\nu(t)\right) + \begin{bmatrix}0_{3\times3}\\ I_{3\times3}\\ 0_{1\times3}\end{bmatrix}\mathbf{a}(t) \tag{5}$$

where the state vector $\begin{bmatrix}\mathbf{r}(t) & \mathbf{v}(t) & \nu(t)\end{bmatrix}^\mathrm{T}$ gathers the position and velocity of the spacecraft with respect to Phobos, as well as the true anomaly of the latter around Mars, and the control vector $\mathbf{a}(t)$ represents any propulsive acceleration generated by the spacecraft in the BCBF frame. It shall be noted that the vector field $\mathbf{f}\left(\mathbf{r}(t),\mathbf{v}(t),\nu(t)\right)$ can become extremely complex since it has to account for: [i] the three gravity forces as per Eq. (3) of Mars on Phobos, of Mars on the spacecraft and of Phobos on the spacecraft, [ii] non-inertial effects due to the rotation of the BCBF frame and [iii] propagation of the true anomaly of Phobos for the computation of its position. For an elaborate discussion on this topic, the reader is referred to Joffre *et al.*[9]

2.2 Candidate guidance architectures

With the "spacecraft dynamics & kinematics" (SDK) block defined as in Sec. 2.1, the high-fidelity D&L simulator depicted in Fig. 3 has been developed, featuring different guidance and control schemes.

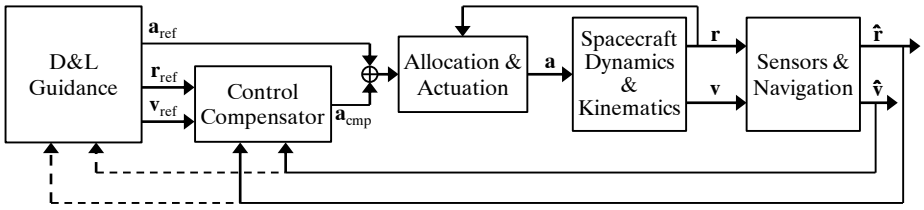

Figure 3: Benchmark architecture (**- - - -** indicates information flow for closed-loop guidance)

In order to accurately model the D&L spacecraft behaviour, as depicted in the figure, the SDK computation is preceded by an "allocation & actuation" block, accounting for thruster realisation errors (e.g., mounting misalignments and limited control authority) and is followed by a "sensors & navigation" module, which implements the algorithms executed to produce relative position and velocity estimates, $\hat{\mathbf{r}}(t)$ and $\hat{\mathbf{v}}(t)$.

In addition, the "D&L guidance" logics is included as required. Two different guidance paradigms are defined: open-loop and closed-loop. These paradigms are detailed in Sec. 2.2.1 and 2.2.2. Finally, to further alleviate trajectory errors, the architecture of Fig. 3 is optionally augmented with a "control compensator", which introduces an additional acceleration vector command $\mathbf{a}_{cmp}(t)$ that compensates for deviations between reference and measured position and velocity. The focus of this paper, however, is not on this compensator and hence its action is not considered for guidance tuning. In fact, in the ideal case, this module has no effect on the system since there are no deviations with respect to the reference trajectory.

2.2.1 Open-loop guidance

Open-loop (or implicit) guidance is employed when a reference trajectory $\{\mathbf{r}_{ref}(t), \mathbf{v}_{ref}(t)\}$ and thruster profile $\mathbf{a}_{ref}(t)$ are generated before, and remain unchanged during the descent. In the case of Phobos, with a complex and poorly-know gravitational field, this approach has been shown not to be robust enough for a successful D&L landing strategy.[9]

For this study, reference trajectories (RTs) were designed by Airbus through the following process: [i] analysis of a set of unstable manifolds originated at Libration Point Orbits (LPOs) in the three-body system that intersect Phobos (Fig. 4a), [ii] selection of the manifolds the reach the moon with higher incidence angle and lower closing speed as initial guesses, [iii] definition of a polynomial acceleration profile aimed at bringing the final closing speed to zero and [iv] optimisation of the initial guesses and acceleration profile via nonlinear programming, with the objective of minimum propellant consumption or ΔV, defined as:

$$\Delta V(t) = \int_0^t \left[\mathbf{a}^{\mathrm{T}}(\tau)\,\mathbf{a}(\tau)\right]^{1/2} \mathrm{d}\tau \tag{6}$$

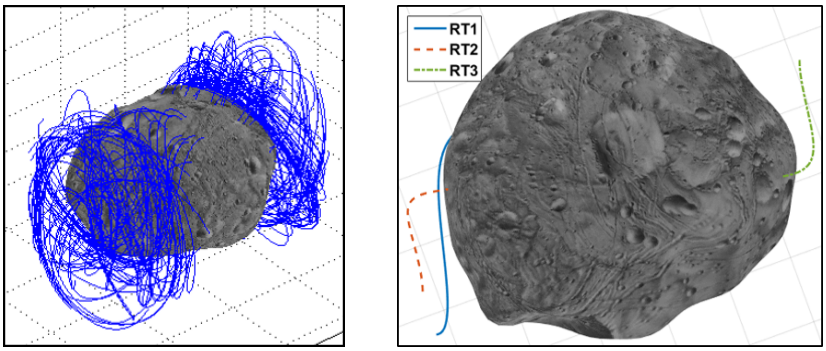

(a) Candidate manifolds (b) Optimised trajectories

Figure 4: Reference D&L trajectory design

For a detailed description on this process, the reader is referred to Joffre *et al.*[9] The three trajectories visible in Fig. 4b will be addressed in this paper, with a stronger emphasis on RT1 to illustrate the proposed tuning methodology.

2.2.2 Closed-loop guidance

Closed-loop (or explicit) guidance refers to the case when the thruster profile is computed in real-time to correct the trajectory based on onboard measurements, as shown in Fig. 3 by the dashed lines. In this case, the "D&L guidance" subsystem is also responsible for the computation of auxiliary variables such as line-of-sight or zero-effort errors.

As mentioned before, although distinct types of closed-loop laws have been identified, it was observed that they share structural commonalities and can be generalised using line-of-sight or zero-effort error kinematics:[13]

$$\mathbf{a}(t) = \begin{bmatrix} k_r & k_v \end{bmatrix} V_c(t) \begin{bmatrix} \dfrac{\mathbf{\Lambda}(t)}{t_{\text{go}}(t)} \\ \dot{\mathbf{\Lambda}}(t) \end{bmatrix} - \phi\, \mathbf{h}\left(\mathbf{\Lambda}(t), \dot{\mathbf{\Lambda}}(t), t_{\text{go}}(t)\right) \tag{7}$$

$$\mathbf{a}(t) = \begin{bmatrix} k_r & k_v \end{bmatrix} \begin{bmatrix} \dfrac{\mathbf{ZEM}(t)}{t_{\text{go}}^2(t)} \\ \dfrac{\mathbf{ZEV}(t)}{t_{\text{go}}(t)} \end{bmatrix} - \phi\, \mathbf{h}\left(\mathbf{ZEM}(t), \mathbf{ZEV}(t), t_{\text{go}}(t)\right) \tag{8}$$

These equations show a fixed structure formed by a linear component, parameterised through gains k_r and k_v, plus a nonlinear function $\mathbf{h}(\cdot)$ weighted by the constant ϕ, which can be introduced to improve robustness properties but will be set to zero from now on, for simplicity. Line-of-sight and zero-effort errors can be directly defined with respect to the landing site or, also for improved robustness, to a set of intermediate waypoints. For this study, the latter option is adopted, using waypoints from the reference trajectories of Fig. 4b.

Depending on the choice of gains $\{k_r, k_v\}$, closed-loop guidance laws may present very different properties. For the case of constrained terminal velocity guidance (CTVG), standard values of {6, -2} for the gains in Eq. (8) can be analytically derived[7,8] by recasting the D&L problem as an optimal control with constrained terminal position and velocity and using the cost function:

$$J(\mathbf{a}(t)) = \frac{1}{2} \int_0^{t_f} \mathbf{a}^{\mathrm{T}}(\tau)\, \mathbf{a}(\tau)\, \mathrm{d}\tau \tag{9}$$

Note that this problem does not represent a direct minimisation of ΔV in Eq. (6), but it is generally easier to solve and provides a representative solution. Furthermore, the derivation is carried out under the assumption of simplified and well-known gravitational fields, which does not hold for the case of Phobos.

The aim of this paper is therefore to revisit and try to improve the standard gain selection for complex and perturbed gravitational environments such as Phobos.

3. Guidance tuning via systematic simulation

This section presents the closed-loop guidance tuning methodology developed via systematic simulation. It starts (Sec. 3.1) with a thorough exposition of the proposed approach and with the results obtained for RT1, followed in Sec. 3.2 by its application to the other two trajectories (recall Fig. 2b). The section concludes with a Monte-Carlo (MC) validation campaign in Sec. 3.3.

3.1 Proposed approach

A successful guidance tuning is always a translation of an appropriate trade-off between acceptable touchdown (position and velocity) accuracy and the total ΔV needed for the D&L manoeuvre. As mentioned before, using results from optimal control theory, standard closed-loop guidance gains can be analytically derived. Nevertheless, these gains are only practical under the assumption of simplified and well-known gravitational fields.

In order to provide not just a systematic tuning methodology in the case of highly complex and perturbed gravitational environments, but also a clear understanding of the aforementioned trade-off, a simulation-based approach is proposed in this paper. This approach relies on the nonlinear high-fidelity simulator introduced in Sec. 2.2 to evaluate three key performance indicators:

- R_c - Target distance (i.e., position error) at touchdown, given by $\|\mathbf{r}_f - \mathbf{r}(t_f)\|$;
- V_c - Closing speed (i.e., velocity error) at touchdown, given by $\|\mathbf{v}_f - \mathbf{v}(t_f)\|$;
- ΔV - Total ΔV, given by Eq. (6) with $t = t_f$.

Also as introduced in Sec. 2.2, the proposed tuning approach is illustrated using the parametric guidance generalisation of Eq. (8) and a set of intermediate waypoints from trajectory RT1. This approach is described in the following paragraphs.

3.1.1 Nominal indicators

The first step is to evaluate the three performance indicators in nominal conditions over a parameter grid of $\{k_r, k_v\}$. This is represented for RT1 by the three plots of Fig. 5. These plots provide a clear visualisation of the tuning trade-off mentioned before. In exactitude, a choice of gains that minimises the touchdown error (either in terms of position and velocity) will maximise the required ΔV and vice-versa.

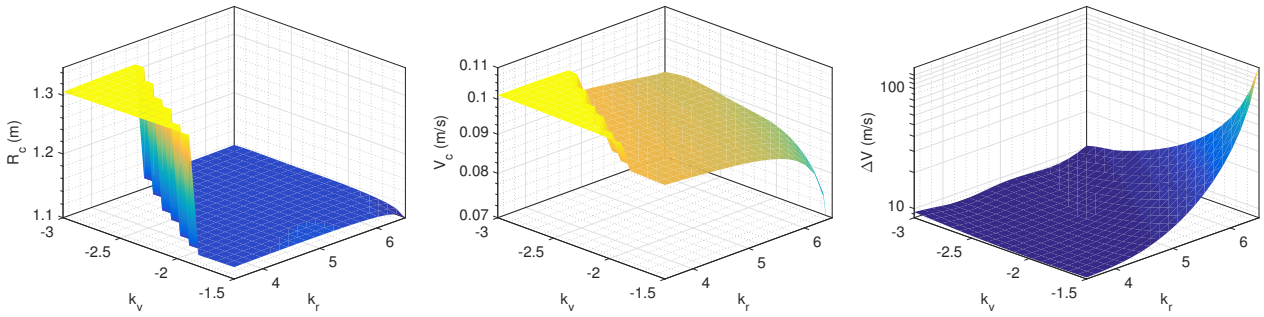

(a) Target distance at touchdown (b) Closing speed at touchdown (c) Total ΔV

Figure 5: Nominal performance indicators at touchdown for RT1

3.1.2 Dispersed indicators

The same principle is then employed to quantify the dispersed performance obtained with each pair $\{k_r, k_v\}$ by analysing the standard deviation of the key indicators for 100 random samples of the 19 uncertain GH coefficients in Eq. (4) with Gaussian distributions. The outcome is provided in Fig. 6, where it is possible to observe that certain guidance solutions are associated with intense indicator peaks, which must evidently be avoided.

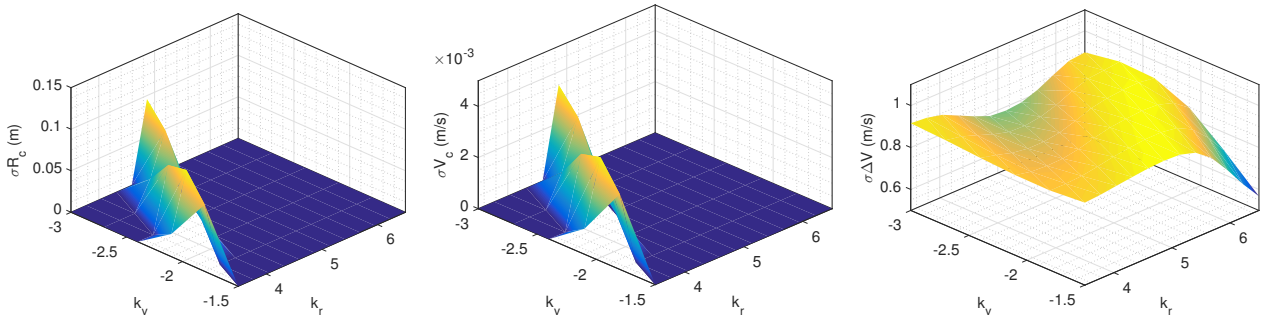

(a) Target distance at touchdown (b) Closing speed at touchdown (c) Total ΔV

Figure 6: Dispersed performance indicators at touchdown for RT1

3.1.3 Trade-off maps

The final step is to generate a tuning trade-off map featuring both nominal and dispersed information by overlapping the contour plots of the previous two figures. Such trade-off map is depicted in Fig. 7 for RT1.

Focusing on Fig. 7a, blue and red solid lines represent respectively the contour plots of closing speed from Fig. 5b and total ΔV from Fig. 5c. Note that target distance could have been used instead of closing speed since their nominal and dispersed trends are similar. As mentioned before, a minimisation of V_c requires an increment of ΔV and vice-versa, but solutions exist such that minor degradations in V_c allow for high ΔV improvements. Furthermore, the map of ΔV has a global minimum (under 8.8 m/s), but it coincides with the area where V_c becomes significantly higher.

For this reason, the transition area lies on a peak of V_c dispersion (from Fig. 6b), which is depicted in the trade-off map of Fig. 7a using dashed black lines. In the same map, the contours of ΔV dispersion (from Fig. 6c) are represented using dashed magenta lines. This plot allows to identify a global maximum (actually very close to the standard gains {6, -2} and marked with a red ×) and a local minimum next to the nominal minimum of ΔV.

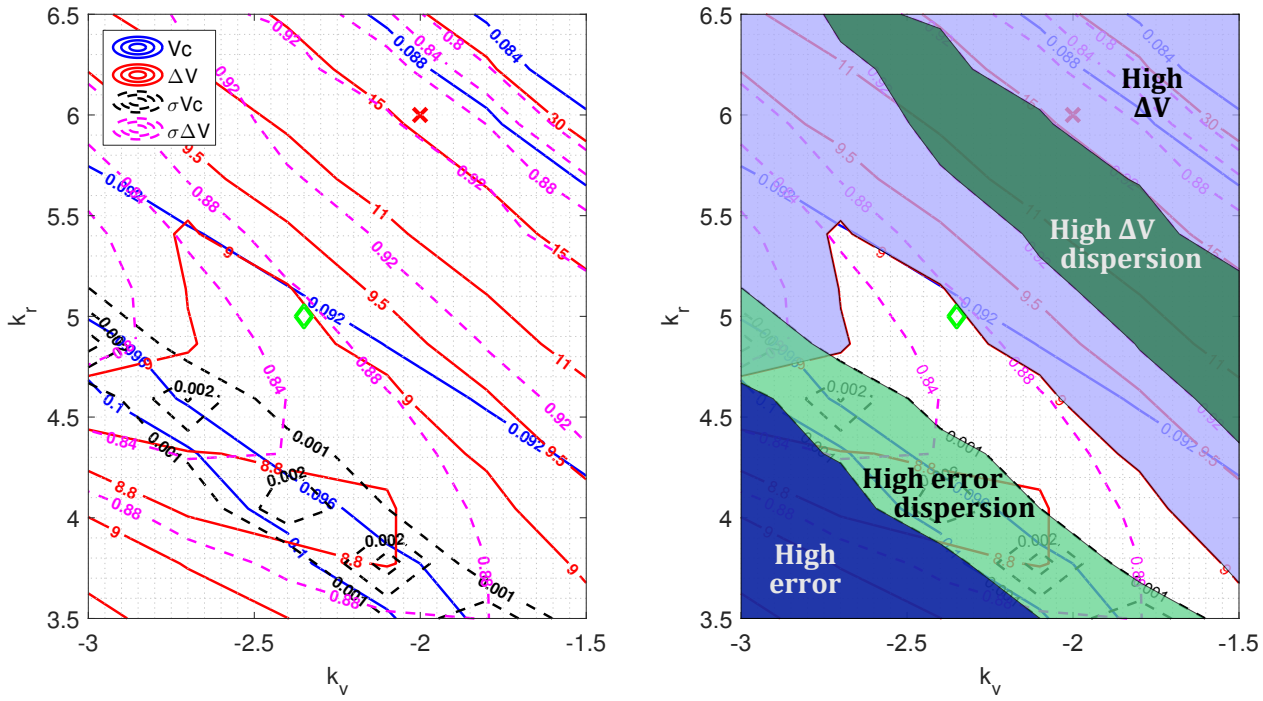

(a) Plain map

(b) Map with undesirable regions

Figure 7: Guidance trade-off map for RT1 (× indicates standard gains, ◇ indicates revised gains)

For an easier visualisation of the observations above, Fig. 7b highlights the undesirable tuning regions of Fig. 7a. This clearly leads to the conclusion that the standard choice of gains is not the most suitable (at least for the studied Phobos mission) since it is associated with relatively high values of both nominal and dispersed ΔV.

Hence, the proposed tuning trade-off process and maps can be systematically employed for a more favourable selection of guidance gains. For example, choosing $\{k_r, k_v\}$={5, -2.35}, marked with a green ◇ in Fig. 7a and 7b, allows ΔV to be reduced from 15.9 to less than 9 m/s while only increasing V_c from slightly more than 0.088 to approximately 0.092 m/s. At the same time, although it does not correspond to the minimum of ΔV dispersion, this choice reduces its value from around 0.9 to less than 0.88 m/s and, most importantly, keeps a safety margin with respect to the peaks of nominal and dispersed V_c.

The exact nominal values can be directly read from the map, but the dispersed indicators shall go through a more extensive Monte-Carlo (MC) validation since, for the sake of computational efficiency, the trade-off map is based on a very limited number (100) of simulations per guidance solution $\{k_r, k_v\}$.

3.2 Applicability to other trajectories

Before stepping into MC validation, however, the applicability of the tuning approach proposed in Sec. 3.1 to other D&L trajectories shall be assessed. Following the same procedure of the latter section, trade-off maps for RT2 and RT3, Fig. 8a and 8b, can be generated. As before, the same standard and revised choices of gains are marked with × and ◇, respectively.

For both trajectories, it can be seen that, similarly to RT1, switching from standard to revised gains results in a large decrease of ΔV (about 3.5 m/s for RT2 and 2.5 m/s for RT3) with a minor increase of V_c (approximately 1 mm/s for both). The main difference between these two trajectories and RT1 is the absence of V_c dispersion peaks (dashed black lines) in the former (in which this indicator is inversely proportional to k_r). This seems to indicate the existence of a terrain hazard in RT1 where the spacecraft collides for certain guidance solutions, which is not the case in RT2 or RT3.

Also, it is possible to verify that, contrary to RT1, the revised choice of gain is not the best for RT2 and RT3 in terms of ΔV dispersion (dashed magenta lines), since it is associated with higher values than the standard gains. However, the impact of this behaviour is much less significant than the nominal ΔV reduction and, for the sake of simplicity, the same revised gains are kept for the remainder of the paper.

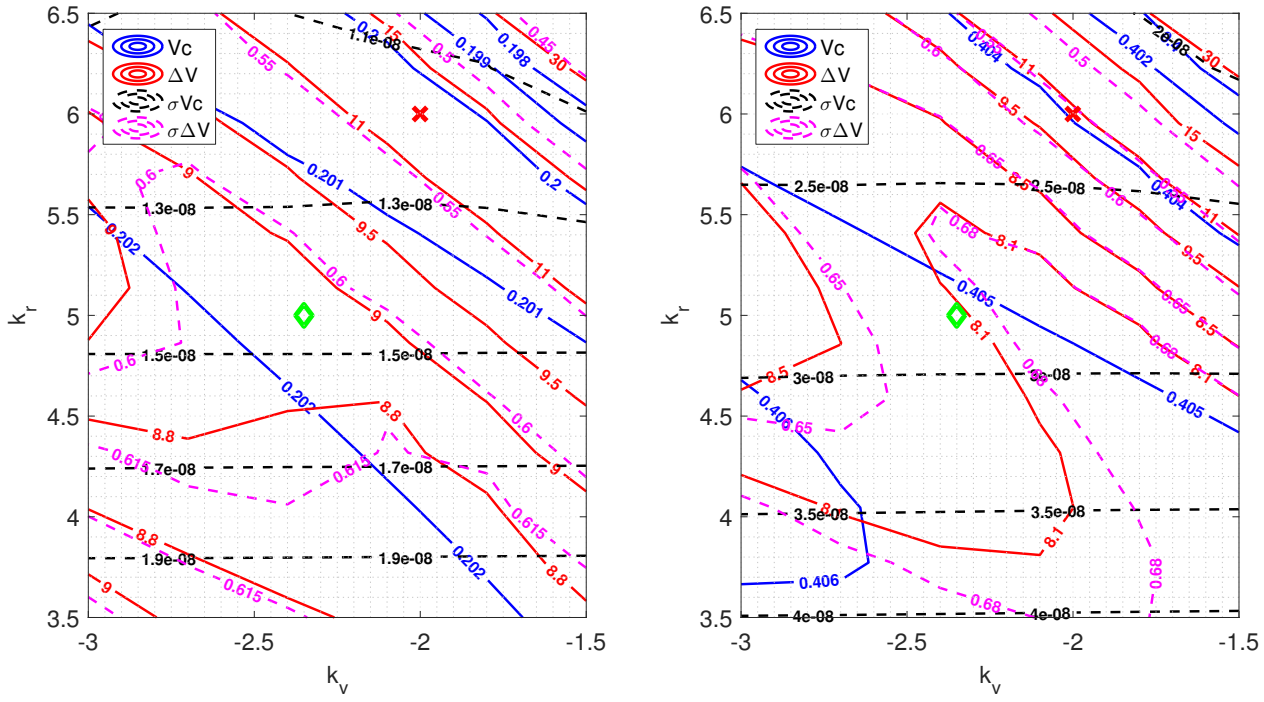

(a) RT2 (b) RT3

Figure 8: Guidance trade-off maps for other trajectories (× indicates standard gains, ◇ indicates revised gains)

For a real-life application, the authors envisage the practical implementation of the proposed tuning methodology as follows:

1. High-fidelity simulation and guidance trade-off maps are generated on ground for a set of candidate D&L trajectories;
2. Once the spacecraft approaches the target and local analyses are carried out, the most suitable reference trajectory can be selected;
3. The most performing tuning selection is then determined before initiating the D&L manoeuvre using the appropriate trade-off map.

The main benefit of this approach is that guidance tuning selection is able to account for the actual ΔV available and acceptable landing accuracy (e.g., based on visual observations) at the time, without involving any major real-time computation.

3.3 Monte-Carlo validation

To validate the results discussed in the previous sections, the revised guidance gains $\{k_r, k_v\}$={5, -2.35} are now tested and compared with the standard tuning selection $\{k_r, k_v\}$={6, -2} using the benchmark introduced in Sec. 2.2. Each guidance tuning is simulated against the same 1000 MC samples of the 19 GH coefficients in Eq. (4) with Gaussian distributions for the three reference trajectories in Fig. 4b (with trade-off maps shown in Fig. 7a, 8a and 8b). As mentioned in Sec. 3.2, the revised gains have been optimised for RT1 but are kept the same for RT2 and RT3 for the sake of simplicity. Moreover, since the focus of this analysis is on the impact of the GH coefficients, no additional perturbations from actuators or navigation are included in the simulations.

The outcomes of this validation campaign are depicted in Fig. 9, with a different column for each reference trajectory and using darker and lighter lines for results using respectively the standard or the revised gains. For each case, the target distance $\|\mathbf{r}_f - \mathbf{r}(t)\|$, closing speed $\|\mathbf{r}_f - \mathbf{r}(t)\|$ and required ΔV are given.

From Fig. 9 it is clear that, for the three trajectories, the revised gain selection results in significant ΔV savings with a minimal impact on position and velocity errors. Since the revised gains have been optimised for RT1, it is natural that ΔV savings are higher for this trajectory than for RT2 and RT3.

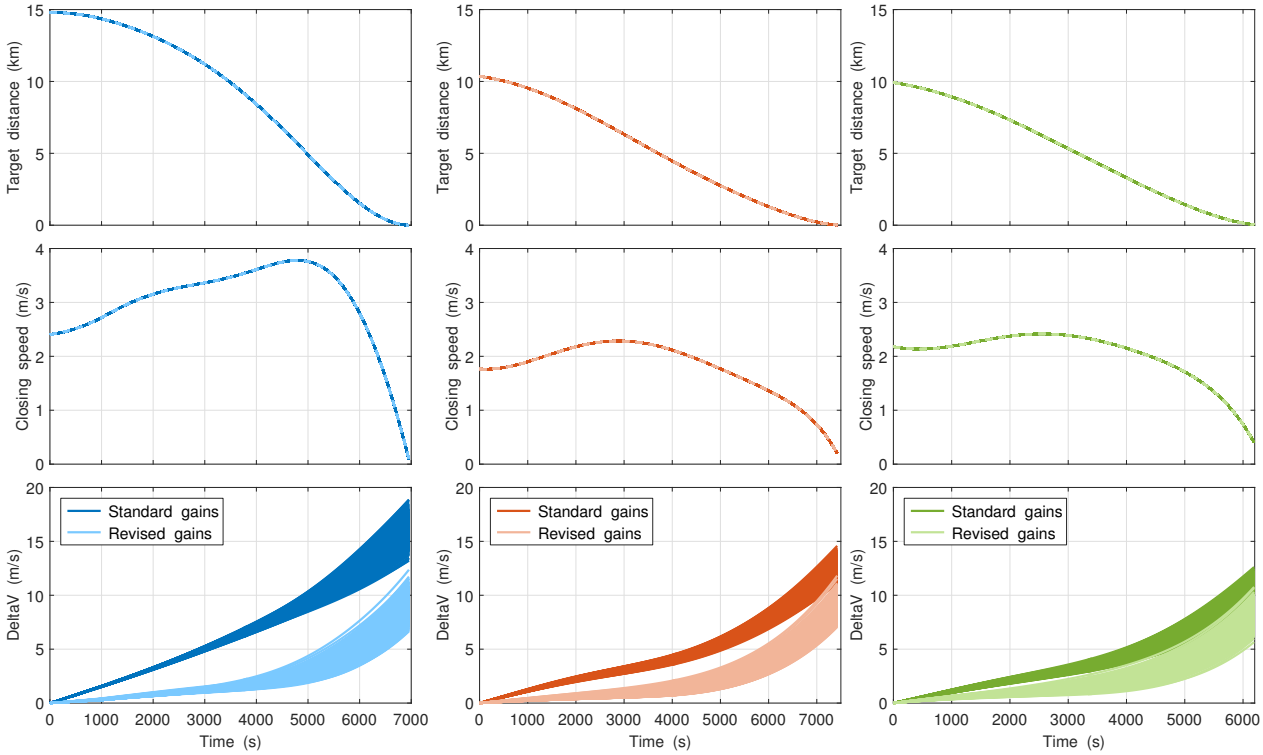

(a) RT1 (b) RT2 (c) RT3

Figure 9: High-fidelity simulation results of 1000 MC runs per trajectory with different gains

For a detailed comparison, the average and standard deviation of the final values encountered for the MC simulations are recorded in Table 1. Note that these indicators are directly related to the ones employed for the generation of the trade-off maps in Sec. 3.1.

Table 1: Performance comparison of 1000 MC runs per trajectory with different gains

	RT1		**RT2**		**RT3**	
With standard gains	Avg.	Std.	Avg.	Std.	Avg.	Std.
R_c (m)	1.118	8.15×10^{-5}	11.949	1.82×10^{-4}	39.053	1.72×10^{-4}
V_c (m/s)	0.089	4.91×10^{-9}	0.200	1.45×10^{-8}	0.404	2.19×10^{-8}
ΔV (m/s)	15.905	9.96×10^{-1}	12.574	6.25×10^{-1}	10.586	7.02×10^{-1}
With revised gains	Avg.	Std.	Avg.	Std.	Avg.	Std.
R_c (m)	1.117	9.80×10^{-5}	11.946	2.19×10^{-4}	39.050	2.07×10^{-4}
V_c (m/s)	0.092	6.32×10^{-9}	0.202	1.76×10^{-8}	0.405	2.64×10^{-8}
ΔV (m/s)	8.819	9.71×10^{-1}	9.009	8.00×10^{-1}	8.073	8.24×10^{-1}

As anticipated from Sec. 3.1 for RT1, the revised gains enable a significant reduction in both average and dispersed ΔV at the expense of a minor increase in average and dispersed velocity error. In fact, in terms of average indicators, a ΔV reduction of 44.5% is achieved with a velocity error increase of only 3.4%. As mentioned before, these indicators can be directly read from the trade-off map of Fig. 7a. On the contrary, the dispersed indicators do not correspond exactly to the values of Fig. 7a because the trade-off map was generated from a smaller number of simulations (100), but the mismatch is also relatively small (about 9%).

At this point, it shall be noted that the non-zero average position and velocity errors, visible in the table but not in Fig. 9, are due to numerical simplifications introduced for the design of the three reference trajectories (recall Sec. 2.2.1).

Similar conclusions then hold for RT2 and RT3: the revised gains enable a significant reduction in terms of average ΔV at the expense of a minor increase in average and dispersed velocity error and also dispersed ΔV, as anticipated from Sec. 3.2. The latter increase is however very small (0.18 m/s for RT2 and 0.12 m/s for RT3, clearly outweighed by the average improvements of 28.5% and 23.7%, respectively) and could have been compensated by a dedicated choice of guidance gains for each trajectory.

With the aforementioned observations in mind, not only does this section validate the proposed guidance tuning methodology, it also confirms that the state-of-practice tuning selection, based on the cost function of Eq. (9) and on the assumption of simplified and well-known gravitational fields, is not fuel-optimal for the case of Phobos.

4. Reconciliation with structured $\mathcal{H}_\infty$ optimisation

This section shows how the guidance tuning methodology proposed in Sec. 3 can reconcile and complement alternative approaches such as the structured $\mathcal{H}_\infty$ optimisation, which is able to explicitly account for uncertainties. The specific interest on structured $\mathcal{H}_\infty$ is further motivated in Sec. 4.1 and the uncertainty modelling process is summarised in Sec. 4.2. A detailed description of guidance tuning via structured optimisation lies outside the scope of this paper, but a brief overview is provided in Sec. 4.3.

4.1 Why structured $\mathcal{H}_\infty$ optimisation?

The closed-loop guidance laws addressed in this paper, see Eq. (8), have a fixed structure parameterised by tuneable gains k_r and k_v, which makes them perfect candidates for the application of the novel structured $\mathcal{H}_\infty$ optimisation paradigm. The capability of this paradigm in taking advantage of state-of-practice guidance structures and industry legacy knowledge is a very important point as it enables the transfer of the tuning approach to industry without representing a disruptive change in the design teams.

In addition to this capability, the application of structured $\mathcal{H}_\infty$ optimisation to the D&L problem offers two other main advantages:

- Being a Robust Control technique[1] it allows to explicitly account for uncertain gravitational environments;
- It is able to directly handle multiple tuning goals and design models[6] thus providing solutions that are valid not only for one, but for a set of operating points in space or reference trajectories.

Naturally, these advantages come at the expense of a challenging (non-smooth) mathematical problem. To solve it, the structured $\mathcal{H}_\infty$ algorithm uses local optimisation methods and relies on multiple runs from random initial conditions to mitigate its local nature, which typically makes its solution non-reproducible. This irreproducibility represents a key issue within industry due to certification concerns and also a breakdown in the tuning learning experience (i.e., the assessment of system behaviour changes due to changes in the posing of the problem).

Despite this challenge, the strenghts mentioned above make structured $\mathcal{H}_\infty$ a very industry-oriented approach and its effectiveness has already been proven through two Space-flown missions[5,11] and more recently in piloted flight tests.[10] Under the scope of planetary D&L, the application presented in Falcoz *et al.*[5] is particularly interesting since it showed how structured $\mathcal{H}_\infty$ was employed for the refinement of the European Rosetta's orbit controller after thruster authority degradation. The revised control gains were uploaded to the spacecraft just before its braking and final insertion manoeuvres with the target comet in May 2014.

As mentioned before, a detailed description of guidance tuning via structured $\mathcal{H}_\infty$ optimisation is not in the scope of this paper, but an overview of preliminary results focused on its reconciliation with the proposed systematic tuning approach is provided in Sec. 4.3. Before stepping into these results, however, Sec. 4.2 introduces how the two features stated above (i.e., ability to account for uncertainties and for multiple points in space) are included within this tuning approach.

4.2 Gravitational uncertainty modelling

The development of models that allow to capture gravitational uncertainty effects is based on the so-called linearised orbital perturbation theory.[2] According to this theory, state and control variables can be defined at different operating points along a given trajectory as the sum of a reference (desired) value and small perturbations (deviations). The dynamics of these perturbations is then approximated by the 1st order terms of the Taylor series expansion of $\mathbf{f}\left(\mathbf{r}(t), \mathbf{v}(t), v(t)\right)$ from Eq. (5) around the reference points:

$$\begin{bmatrix}\delta\dot{\mathbf{r}}(t)\\ \delta\dot{\mathbf{v}}(t)\\ \delta\dot{\nu}(t)\end{bmatrix} = J_{\mathbf{f}}(t)\begin{bmatrix}\delta\mathbf{r}(t)\\ \delta\mathbf{v}(t)\\ \delta\nu(t)\end{bmatrix} + \begin{bmatrix}0_{3\times3}\\ I_{3\times3}\\ 0_{1\times3}\end{bmatrix}\delta\mathbf{a}(t) \tag{10}$$

where the Jacobian matrix given by:

$$J_{\mathbf{f}}(t) = \left[\frac{\partial\mathbf{f}}{\partial\mathbf{r}} \quad \frac{\partial\mathbf{f}}{\partial\mathbf{v}} \quad \frac{\partial\mathbf{f}}{\partial\nu}\right]\Bigg|_{\substack{\mathbf{r}=\mathbf{r}_{\text{ref}}(t)\\ \mathbf{v}=\mathbf{v}_{\text{ref}}(t)\\ \nu=\nu_{\text{ref}}(t)}} \tag{11}$$

is computed via finite differences due to the complexity of $\mathbf{f}\left(\mathbf{r}(t), \mathbf{v}(t), \nu(t)\right)$. Performing this linearisation at different instants of time t_i, $i = \{1, \ldots, N\}$ along a reference trajectory allows to generate a set of linear time-invariant (LTI) "spacecraft dynamics & kinematics" (SDK) models $G^i_{\text{SDK}}(\text{s})$, with the following state-space description:

$$\left[\begin{array}{c}\dot{\mathbf{x}}_{\text{SDK}}(\text{s})\\ \hline \delta\mathbf{r}(\text{s})\\ \delta\mathbf{v}(\text{s})\end{array}\right] = \left[\begin{array}{cc|c} & & 0_{3\times3}\\ & J^i_{\mathbf{f}} & I_{3\times3}\\ & & 0_{1\times3}\\ \hline I_{6\times6} & 0_{6\times1} & 0_{6\times3}\end{array}\right]\left[\begin{array}{c}\mathbf{x}_{\text{SDK}}(\text{s})\\ \hline \delta\mathbf{a}(\text{s})\end{array}\right] \tag{12}$$

where $J^i_{\mathbf{f}} = J_{\mathbf{f}}(t_i)$ and $\mathbf{x}_{\text{SDK}}(\text{s})$ is the internal state vector.

As introduced in Sec. 2.1, 19 out of the 28 GH coefficients are highly inaccurately known. This means that the computation of $J^i_{\mathbf{f}}$ and thus the description of $G^i_{\text{SDK}}(\text{s})$ in Eq. (12) is subject to a high level of uncertainty. To capture the effect of this uncertainty, a mathematical representation known as linear fractional transformation (LFT) is employed.[3,14] LFTs are particularly attractive due to their extreme modularity and because typical algebraic operations (e.g., inverse, cascade, parallel and feedback connections) preserve the LFT structure. Therefore, in an interconnected system, it is common to isolate what is known as an LTI system $M(\text{s})$ and gather all the "troublemaking" (uncertain, time-varying or nonlinear) components into an operator $\Delta_{\text{x}} = \text{diag}\left(\delta_{\text{x}_1}, \delta_{\text{x}_2}, ..., \delta_{\text{x}_n}\right)$, bounded as $\|\Delta_{\text{x}}\|_\infty \leq 1$. To build representative LFT models of $G^i_{\text{SDK}}(\text{s})$, the following procedure has been adopted:

1. In order to minimise the size of the resulting LFT model, only the GH coefficients with higher impact on $J^i_{\mathbf{f}}$ are selected and denoted ρ_{GH}. For this choice, two distinct criteria are applied: impact of each coefficient on the nonlinear simulation of Eq. (5) and relative weight of each coefficient on dedicated interpolations (refer to next step).

2. Once the set of uncertainties is selected, an appropriate number of dispersed samples is generated and the Jacobian matrix in Eq. (11) is evaluated for each sample. Depending on the dispersion ranges considered, models with different levels of conservativeness can be obtained. For each case, a matrix with polynomial dependence on the uncertain parameters $J^i_{\mathbf{f}}(\rho_{\text{GH}})$ is then interpolated. This task is accomplished using the orthogonal least-squares approximation routine of ONERA's "Apricot" library.[12]

3. The final step consists in converting the LTI system of Eq. (12) with $J^i_{\mathbf{f}}(\rho_{\text{GH}})$ into an LFT. This is also an embedded capability of the "Apricot" library, which adjusts the necessary repetitions of each coefficient in ρ_{GH} to meet a pre-specified approximation error. Finally, the accuracy of the LFTs is verified by comparing frequency response samples obtained from an LFT and from equivalently dispersed LTI realisations.

   This procedure is then repeated for every time instant t_i of interest along one or more trajectories.

4.3 Preliminary results

The main difficulty in the application of structured $\mathcal{H}_\infty$ optimisation to the D&L problem lies on its formulation as an $\mathcal{H}_\infty$ problem. As introduced in Sec. 2.2.2, state-of-practice guidance solutions have been found by recasting it as an optimal control problem with the cost function given in Eq. (9) and constrained terminal position and velocity. This is substantially different from the structured $\mathcal{H}_\infty$ problem, which aims at minimising the induced $\mathcal{H}_\infty$-norm of pre-specified input-output control channels:

$$\min_{k_r, k_v} \left\{\max\left(\|M_1(\text{s})\|_\infty, \ldots, \|M_N(\text{s})\|_\infty\right)\right\} \tag{13}$$

where $M_i(\text{s})$, with $i = \{1, \ldots, N\}$, are linear representations of the system dynamics at different operating points along one or more reference trajectories.

The linear representations $M_i(s)$ include not only the SDK dynamics, but also algorithms for the estimation of apparent gravity and zero-effort errors and for the computation of guidance commands as per Eq. (8). The SDK dynamics can be conveniently replaced by the orbital perturbation model of Eq. (12) and the remaining interconnections can be implemented in Simulink and retrieved using its `slTuner` interface. The latter interface is part of MATLAB from 2014 onwards and allows to automatically create linear models of Simulink systems that can be employed for control tuning. Here, it is adopted to obtain the linear representations $M_i(s)$ containing the gains k_r and k_v as tuneable parameters.

Moreover, with `slTuner`, the different points $i = \{1, \ldots, N\}$ where $M_i(s)$ is defined can be specified using the `findop` function and the effect of gravitational uncertainties can be explicitly accounted for by injecting the LFTs created in Sec. 4.2 through its `BlockSubs` field. A detailed explanation on this process and on the specification of adequate control channels is outside the scope of the paper, but the Simulink model adopted is depicted in Fig. 10.

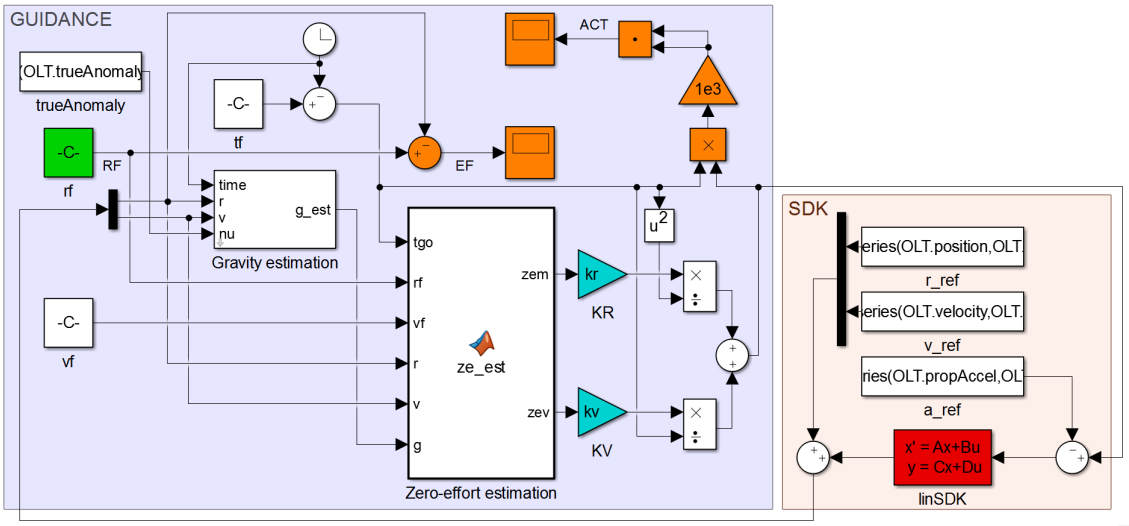

Figure 10: Simulink model for structured guidance tuning

With all the system interconnections and linear representations properly defined, the new tuning goals can be specified and the optimisation problem can be solved. Following the same reasoning of Sec. 3.1, two competing tuning goals are addressed: *accuracy* (minimising touchdown error) and *efficiency* (minimising propellant consumption). In order to exploit the underlying trade-off between them, the optimisation is performed for different weighted combinations of the two requirements. Once again, a thorough description of this process is outside the scope of the paper, but an overview of preliminary results is illustrated in Fig. 11, over the trade-off map of RT1 (from Fig. 7).

The latter figure, in addition to the information introduced in Sec. 3.1, shows two cyan lines: a continuous line representing the $\{k_r, k_v\}$ solution under nominal conditions and a dashed line when the LFT models are considered. On each line, intermediate points indicate the corresponding combination of tuning goals, ranging from *efficiency* only at the bottom of the plot to *accuracy* only at the top.

Between the two extremes, the standard tuning selection given by the red $\times$ is retrieved for a combination of about 85% *accuracy* / 15% *efficiency* for the case of nominal conditions, the same under which the standard gains have been analytically derived. Results using the LFT models show a similar trend, but shifted towards the top right corner of the plot, which is also consistent with the trade-off map of Fig. 7 since the tuning solutions move away from the dispersion peaks of both touchdown error and total ΔV.

The preliminary results in this section confirm that this formulation is able to successfully recover the standard guidance tuning insights. However, as demonstrated by the trade-off map and systematic tuning methodology proposed before, more performing guidance solutions do exist but are not captured using the structured $\mathcal{H}_\infty$ approach due to the high nonlinearity of the system. This represents the main limitation of the approach and thus one of the most relevant topics to be further investigated.

5. Conclusions

This paper proposes a systematic tuning methodology for closed-loop Space descent & landing (D&L) guidance laws. The proposed methodology employs a systematic evaluation of high-fidelity models to generate trade-off maps that provide clear performance and robustness quantifications of candidate guidance solutions.

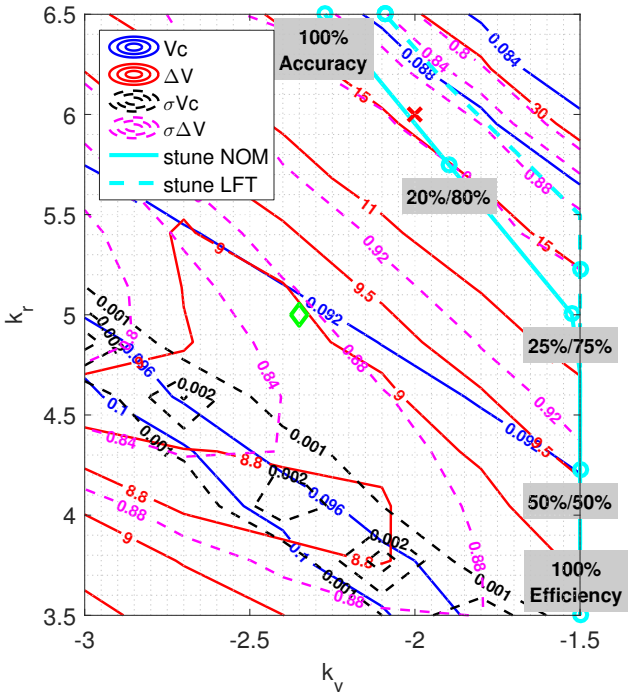

Figure 11: Visualisation of preliminary tuning results over trade-off map

The ability to account for nonlinear and uncertain dynamics is a key aspect of this methodology, which is particularly important when targeting planetary bodies with complex and uncertain environments. In fact, it is shown that, for a landing on Phobos, propellant consumption savings of around 40% could be achieved (for similar touchdown errors) compared to state-of-practice tuning selections derived under the assumption of simplified and well-known gravitational fields.

In addition, trade-off maps can be generated before the D&L mission but only applied once the spacecraft approaches the target body, having in consideration the actual propellant available and without the need for expensive computations, which makes this approach very industry-oriented. Also with this issue in mind, the project under which this study was developed is addressing the applicability of structured $\mathcal{H}_\infty$ optimisation to exploit the fixed structure of D&L guidance laws.

Preliminary results are presented in this paper regarding the reconciliation and complementarity of the two methodologies, but research on this topic is still ongoing. This is mostly related to the fact that, although the state-of-practice tuning selections could be recovered by the structured $\mathcal{H}_\infty$ approach, superior guidance solutions, identified with trade-off maps, could not be captured due to the highly nonlinear dynamics of the problem.

References

[1] P. Apkarian, M. Dao, and D. Noll. Parametric robust structured control design. *Transactions on Automatic Control*, 60(7):1857–1869, 2015.

[2] R. Battin. *An Introduction to the Mathematics and Methods of Astrodynamics*. AIAA Education Series, 1st edition, 1987.

[3] J. Doyle, A. Packard, and K. Zhou. Review of LFTs, LMIs and μ. In *The 30th IEEE Conference on Decision and Control*, Brighton, UK, Dec 11–13 1991.

[4] B. Ebrahimi, M. Bahrami, and J. Roshanian. Optimal sliding-mode guidance with terminal velocity constraint for fixed-interval propulsive maneuvers. *Acta Astronautica*, 62(10):556–562, 2008.

[5] A. Falcoz, C. Pittet, S. Bennani, A. Guignard, C. Bayart, and B. Frapard. Systematic design methods of robust and structured controllers for satellites. *Space Journal*, 7(3):319–334, 2015.

[6] P. Gahinet and P. Apkarian. Structured $\mathcal{H}_\infty$ Synthesis in MATLAB. In *The 18th IFAC World Congress*, Milan, Italy, Aug 28–Sep 2 2011.

[7] Y. Guo, M. Hawkins, and B. Wie. Optimal Feedback Guidance Algorithms for Planetary Landing and Asteroid Intercept. In *The 2011 AAS/AIAA Astrodynamics Specialist Conference*, Girdwood, AK, Jul 31–Aug 4 2011.

[8] M. Hawkins, Y. Guo, and B. Wie. Spacecraft Guidance Algorithms for Asteroid Intercept and Rendezvous Missions. *International Journal of Aeronautical and Space Sciences*, 13(2):154–169, 2012.

[9] E. Joffre, M. Zamaro, N. Silva, A. Marcos, P. Simplício, and B. Richardson. Landing on Small Bodies Trajectory Design, Robust Nonlinear Guidance and Control. In *The 27th AAS/AIAA Spacefilght Mechanics Meeting*, San Antonio, TX, Feb 5–9 2017.

[10] A. Marcos and M. Sato. Flight Testing of a Structured H-infinity Controller: a EU-Japan Collaborative Experience. In *The 1st IEEE Conference on Control Technology and Applications*, Kohala Coast, HI (pending acceptance), Aug 27–30 2017.

[11] C. Pittet and P. Prieur. Structured accelero-stellar estimator for MICROSCOPE drag-free mission. In *The 3rd CEAS EuroGNC Conference*, Toulouse, France, Apr 13–15 2015.

[12] C. Roos, G. Hardier, and J-M. Biannic. Polynomial and rational approximation with the APRICOT Library of the SMAC toolbox. In *The 2014 IEEE Conference on Control Applications*, Antibes, France, Oct 8–10 2014.

[13] P. Simplício, A. Marcos, E. Joffre, M. Zamaro, and N. Silva. Parameterised Laws for Robust Guidance and Control of Planetary Landers. In *The 4th CEAS EuroGNC Conference*, Warsaw, Poland, Apr 25–27 2017.

[14] K. Zhou, J. Doyle, and K. Glover. *Robust and Optimal Control*. Prentice-Hall, 1st edition, 1995.